J. Fluid Mech. (1988), *vol.* 192, *pp.* 561–575
Printed in Great Britain

A note on vortex shedding from axisymmetric bluff bodies

By PETER A. MONKEWITZ

Department of Mechanical, Aerospace and Nuclear Engineering, University of California, Los Angeles, CA 90024, USA

(Received 10 June 1987 and in revised form 11 December 1987)

The linear parallel and incompressible stability of a family of axisymmetric wake profiles is studied in the range of Reynolds numbers where helical vortex shedding from bluff bodies of revolution is observed. The family of mean flow profiles allows for the variation of the wake depth as well as for a variable ratio of wake width to mixing-layer thickness. It is found that, even without reverse flow, the first helical mode is absolutely unstable in the near wake for Reynolds numbers, based on wake diameter and free-stream velocity, in excess of 3.3×10^3. A survey of the region of local absolute instability as a function of profile parameters and Reynolds number suggests that the large-scale helical vortex shedding, which is observed between Reynolds numbers of 6000 and 3×10^5 for spheres, may be 'driven' by a self-excited oscillation in the near wake.

1. Introduction

The present study has been stimulated by the recent advances in the understanding of vortex shedding from two-dimensional bluff bodies, notably its relation to stability theory. Experimentally, Mathis, Provansal & Boyer (1984) and Strykowski (1986) have shown by ingenious transient measurements that the Kármán vortex street behind a circular cylinder is the nonlinear (saturated) end product of a *self-excited*, i.e. temporally growing, global wake instability and not a spatial response to continuously supplied upstream disturbances. This behaviour of the two-dimensional wake has been related to the existence of a region of local absolute instability in the near wake by, among others, Koch (1985), Monkewitz & Nguyen (1987) and Monkewitz (1988).

In the axisymmetric wake behind spheres, organized vortex shedding has been observed while the boundary layer on the sphere is laminar. Early evidence of vortex shedding has been reviewed by Torobin & Gauvin (1959). Achenbach (1974) then clearly identified two different modes of shedding: a shear-layer mode, dominant at Reynolds numbers R_D (based on sphere diameter and free-stream velocity) between about 400 and 6000 and characterized by a Strouhal number that increases with Reynolds number, and a second mode of shedding, dominant between Reynolds numbers R_D of 6000 and 3×10^5, which is distinguished by an approximately constant and well-defined Strouhal number. The vorticity in the latter mode was shown by Achenbach (1974), Pao & Kao (1977), Taneda (1978) and Ilegbusi & Spalding (1984) to be shed in the form of one helix or a pair of counter-rotating helices. As in the case of the circular cylinder in a cross-flow, the vigorous vortex shedding in this Reynolds-number range appears to coincide with an increase of the drag coefficient c_D above a hypothetical 'smooth' $c_D(R)$ curve (see Schlichting 1968,

figures 1.4 and 1.5; and Achenbach 1972). In view of the above experimental findings, it makes sense to investigate how far the similarity to the cylinder wake extends, i.e. whether the helical vortex shedding in the axisymmetric wake is also possibly related to an absolute instability.

The concept of absolute versus convective instability has been introduced by Briggs (1964), Lifshitz & Pitaevskii (1981) and Bers (1975). Recent reviews of the topic have been given by Pierrehumbert (1984), Huerre & Monkewitz (1985), Bechert (1985), Huerre (1987) and Monkewitz & Nguyen (1987). In short, the terms absolute and convective describe the behaviour of the impulse response of an unstable medium. If an impulsively generated small-amplitude transient contaminates the entire (parallel) flow, it is termed absolutely unstable. In this case, a mode with zero group velocity that grows in time, i.e. is self-excited, eventually dominates the (linear) response. If, on the other hand, the transient or wavepacket is convected away from the source and leaves the flow ultimately undisturbed, one speaks of convective instability. It is readily noted that this distinction depends on the frame of reference. However, in practical problems, where for instance solid boundaries are present, there is always a distinguished frame of reference relative to which the nature of the instability has to be considered (Lifshitz & Pitaevskii 1981).

In flows that evolve spatially, the efforts to relate self-excited (absolute) local instabilities to the vortex shedding from bluff bodies in particular are met with a serious difficulty. At each downstream location within an absolutely unstable region a different local mode has zero group velocity. The central issue, then, is which of these local modes, if any, corresponds to the observed global response, that is, the large-scale vortex shedding in the present situation. One approach in this situation is to formulate *ad hoc* global mode selection criteria on the basis of experimental data (see the review of such criteria by Monkewitz & Nguyen 1987). Another approach has been taken by Chomaz, Huerre & Redekopp (1988) who investigated a one-dimensional model problem described by the Ginzburg–Landau equation, in which only one space coordinate in the mean flow direction is retained to allow for non-parallel effects. Their main findings can be summarized as follows. When investigating global instability modes of their non-parallel system, they found that local absolute instability is *necessary but not sufficient* for a global mode to become self-excited, i.e. to grow in time. They show that the region of local absolute instability has to reach a finite critical size, which depends on the problem at hand, before self-excitation is achieved. In practice this means that the first appearance of local absolute instability in a flow is not expected to produce any discernible effect. It is only the global transition at a higher value of the control parameter (the Reynolds number in the present case) that manifests itself.

In showing that a region of local absolute instability exists in the axisymmetric wake, this paper therefore raises the possibility that the observed helical vortex shedding is driven by a self-excited 'wavemaker' in the near wake. Proof, however, will have to come from transient experiments similar to the ones of Mathis *et al.* (1984). In addition, the following results can possibly serve to find the vortex shedding frequency: The examples presented by Chomaz *et al.* (1988) as well as the experiments of Mathis *et al.* (1984) and Strykowski (1986) appear to indicate that the frequency of a saturated global mode is close to one of the frequencies of the linear modes in the flow which have both zero group velocity and a positive temporal amplification rate.

2. A family of wake profiles and the determination of the absolute or convective nature of their instability

A two-parameter family of axisymmetric wake profiles $U(r)$, which is defined by equation (1) and has already been used by Monkewitz & Sohn (1986), is considered for the present study. U thereby represents a parallel mean flow in the x- or streamwise direction and r is the radial coordinate. Throughout the paper, velocities are made non-dimensional with the average mean velocity $\bar{U}^* = \frac{1}{2}[U_c^* + U_{max}^*]$, where an asterisk denotes a dimensional quantity, $U_c^* = U^*(r = 0)$ is the centreline velocity and U_{max}^* is the maximum mean velocity found at $r = \infty$ for the profiles (1). Lengths are made non-dimensional with the local wake radius b^* which is defined by $U^*(b^*) = \bar{U}^*$. Note that the Reynolds number R, used in the following, will therefore be different from the usual R_D which is based on the body diameter D^* and the free-stream velocity.

$$U(r) = 1 - \Lambda + 2\Lambda F(r), \tag{1}$$

$$\Lambda \equiv \frac{U_c^* - U_{max}^*}{U_c^* + U_{max}^*},$$

$$F(r) \equiv \{1 + [\exp(\ln 2\, r^2) - 1]^N\}^{-1}.$$

Above, the two profile parameters are the velocity ratio Λ and the 'shape parameters' N. Λ thereby controls the depth of the wake with $\Lambda = -1$ corresponding to zero centreline velocity. The shape parameter N, on the other hand, controls the ratio of mixing-layer thickness to wake width and can be varied between $N = \infty$ to define a top-hat wake bounded by a cylindrical vortex sheet and $N = 1$ which corresponds to a Gaussian far-wake profile. Figure 1 shows the normalized profile $F(r)$ for several N. The maximum slope thickness or vorticity thickness δ_ω of the mixing layer on this figure is asymptotically given by

$$\delta_\omega \sim [N \ln 2]^{-1} \quad N \to \infty. \tag{2}$$

A comparison of figure 1 with the experimental data of Fail, Lawford & Eyre (1959), Carmody (1964) and Scholz (1986) in the wake of a circular disk, and the measurements of Riddhagni, Bevilaqua & Lykoudis (1971) behind a sphere shows that the expression (1) is well suited to fit actual wake profiles. Even close to the body, where profiles commonly have a velocity overshoot at the edge of the wake, the results of Monkewitz (1988) for the two-dimensional case suggest that the stability characteristics of the actual profiles and the corresponding profiles (1) match very closely as long as U_{max}^* instead of $U^*(r = \infty)$ is used in the non-dimensionalization. However, in order to allow the applicaion of the following results to a variety of axisymmetric wakes, no specific form of $N(x; R)$ and $\Lambda(x; R)$ will be specified. Hence N, Λ and R will be treated as independent parameters.

The viscous linear stability of the parallel velocity field (1) is now investigated. At the Reynolds numbers of interest the mixing layer leaving the body is initially laminar such that no difficulty of interpretation arises. Further downstream, in addition to the 'large-scale structures' under consideration, small-scale turbulence will generally be present. For this case Strange & Crighton (1983, paragraph 2) use a triple decomposition into ensemble mean, 'large-scale structure' and 'random turbulence' to show that the initial evolution of large-scale features is still correctly modelled by the laminar small-disturbance equations under the following conditions: First, the scale of the instability must be much larger than the scale of the random turbulence; and second, the random turbulence must either be weak (of the same

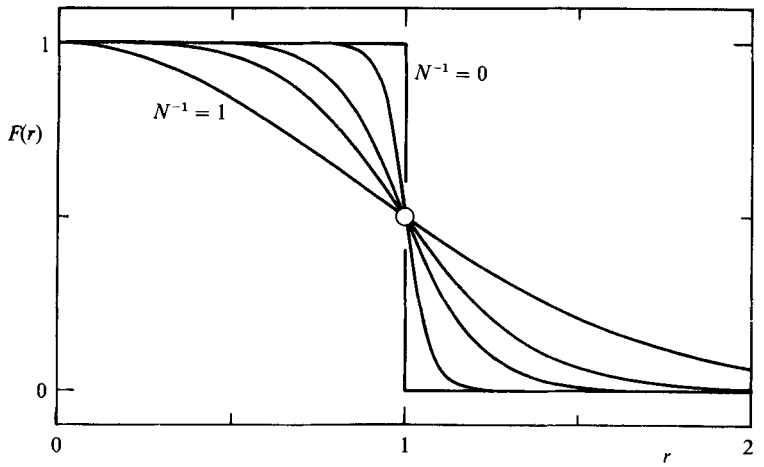

FIGURE 1. Normalized velocity profile $F(r)$, defined by equation (1), for $N^{-1} = 1$, 0.5, 0.3, 0.1, and 0.

order as the instability) or decorellated from the instability on long timescales. Disturbances are, as usual, introduced in the normal mode form

$$q(x, r, \theta, t) = \sum_{m=0}^{m=\infty} \hat{q}_m(r) \exp(\mathrm{i}kx + \mathrm{i}m\theta - \mathrm{i}\omega t), \tag{3}$$

where q represents any disturbance quantity, k is the axial and m the azimuthal wavenumber, and ω is the frequency of the disturbance. The dispersion relation $k(\omega; m)$ is determined by solving the (incompressible) Orr–Sommerfeld equation in cylindrical coordinates, listed in the Appendix for both infinite and finite Reynolds number. For this, a shooting algorithm has been implemented. To ensure adequate accuracy in all cases, including the ones with thin mixing layers, the equations were integrated from $r = \infty$ and from the wake centreline $r = 0$, and the solutions were matched at the centre of the mixing layer $r = 1$. For the numerical integration a standard fourth–fifth-order Runge–Kutta–Fehlberg scheme with stepsize control was used. Following Monkewitz (1978), solutions were kept linearly independent by pseudo-orthogonalization. Good initial guesses for the eigenvalues were obtained from the inviscid calculations.

The absolute or convective nature of the instability was investigated using the Briggs–Bers criterion which requires the determination of the temporal growth rate of the dominant discrete mode at the location of an impulse source. From the analysis of the large-time asymptotic impulse response (see e.g. Huerre & Monkewitz 1985), it follows that this mode has zero group velocity $\mathrm{d}\omega/\mathrm{d}k = 0$. Hence it is associated with a saddle point k^0 of the dispersion relation $\omega(k)$ in the complex k-plane around which $\omega(k)$ has the Taylor expansion

$$\omega = \omega^0 + \tfrac{1}{2}(k - k^0)^2 \frac{\mathrm{d}^2\omega}{\mathrm{d}k^2}(\omega^0). \tag{4}$$

In the ω-plane, $k(\omega)$ has therefore in general a branch point of order two at ω^0. If this branch point lies in the upper complex half-plane, i.e. if the *absolute growth rate* $\mathrm{Im}[\omega^0]$ is positive, one has absolute instability provided the branch point results from the coalescence of a downstream and upstream mode. In technical terms this

means that the maps $k^+(\omega)$ and $k^-(\omega)$ of contours parallel to the real ω-axis must separate into the upper and lower half of the complex k-plane respectively when these contours in the ω-plane are placed sufficiently above the branch point ω^0 (see Huerre & Monkewitz 1985, figure 2 in particular). This condition is the same as the so-called pinching requirement for the integration contour of the 'wavepacket integral' in the k-plane (see any of the references discussing absolute instability). A verification of this requirement in one representative case is shown in the next section as figure 4.

To computationally determine the location of the branch point ω^0 or saddle point k^0, it is however not necessary to obtain complete maps of $k(\omega)$. While Deissler (1987) chose to fit the expression (4) to three eigenvalues $\omega(k^{(i)})$ in order to extrapolate k^0, the analogous procedure in the ω-plane is used for this study. For two $\omega^{(i)}$ the eigenvalues $k^+(\omega^{(i)})$ and $k^-(\omega^{(i)})$ on both Riemann sheets emanating from the branch point ω^0 are computed and the following expression is fitted to these four eigenvalues (see also Monkewitz & Sohn 1986):

$$k^{\pm}-k^0 = \pm s(\omega-\omega^0)^{\frac{1}{2}}+l(\omega-\omega^0). \tag{5}$$

That is, the constants s and l as well as k^0 and ω^0 are determined. Then two new frequencies $\omega^{(i)}$ are chosen closer to the extrapolated branch point ω^0 and the procedure is repeated until both ω^0 and k^0 become stationary (to three significant digits or better).

3. Survey of absolute instability boundaries

As a first step the absolute growth rate $\mathrm{Im}[\omega^0]$ has been explored as a function of the inverse shape parameter N^{-1} for $\Lambda = -1$, infinite Reynolds number, and azimuthal wavenumbers $m = 0$, 1, and 2. For all these cases, both ω^0 and k^0 are shown on figure 2. For $m = 0$ and $m = 2$ the calculations were terminated when ω^0/k^0 became real and a critical layer formed. Hence they do not cover the whole range of N on figure 2. The choice of the abscissa on this graph facilitates its interpretation as N^{-1} is directly proportional to the mixing-layer thickness for large N (equation (2)). In view of the experimental observations it is encouraging that only the first helical mode $m = 1$ is found to have a positive absolute growth rate between $N = 4.72$ and $N = 2.57$. In support of the work by Sato & Okada (1966), the far-wake profile with $N = 1$ is found to be convectively unstable (even for considerable reverse flow on the centreline as shown on figure 5). In the following, the investigation will therefore concentrate on this $m = 1$ mode.

Next, the transition from convective to absolute instability has been investigated as a function of Reynolds number and shape parameter N for the case of zero centreline velocity $\Lambda = -1$ and of $\Lambda = -1.1$ corresponding to a reverse flow on the centreline of 5% of the free-stream velocity. On figure 3, the Reynolds number $R_{c\,A}$ characterizing the transition to (local) absolute instability is plotted as a function of the inverse shape parameter N^{-1}. On the boundary curves $R_{c\,A}(1/N)$ the absolute growth rate $\mathrm{Im}[\omega^0]$ is zero. Above these curves, i.e. for $R > R_{c\,A}$, one finds absolute instability, while parameter values below the boundary curves correspond to convective instability or to a stable flow. From figure 3 it is seen that the minimum $R_{c\,A,\,\min}$ depends strongly on the velocity ratio with $R_{c\,A,\,\min}(\Lambda = -1, N = 3.2) = 8.2 \times 10^2$ and $R_{c\,A,\,\min}(\Lambda = -1.1, N = 3) = 59$. On the other hand, the shape parameter N at which the minimum $R_{c\,A}$ is reached, appears quite insensitive to Λ

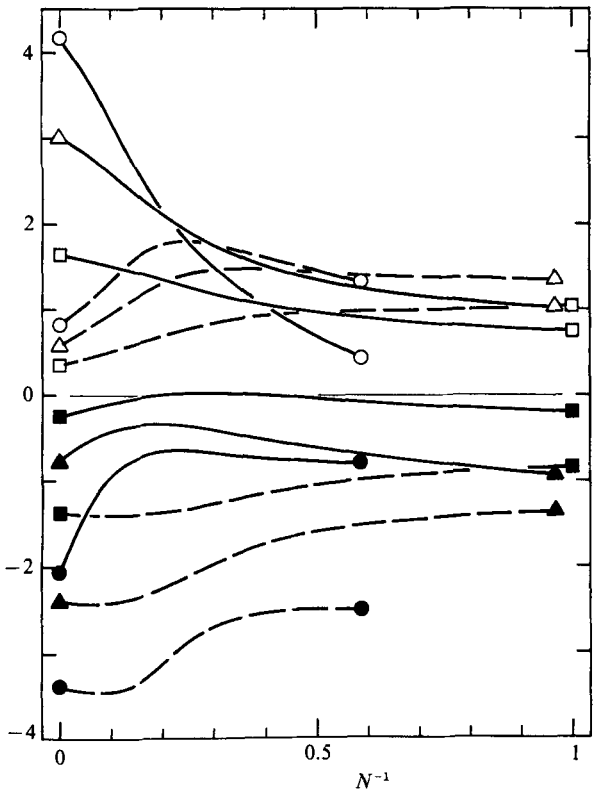

FIGURE 2. Branch point ω^0 (———) and corresponding saddle point k^0 (— — —) versus N^{-1} for $\Lambda = -1$, $R = \infty$, and $m = 0$ (○), $m = 1$ (□), $m = 2$ (△). Open symbols denote real parts and solid symbols imaginary parts.

and has a value of approximately $N \approx 3$. This N corresponds to a profile that has a region of constant velocity over about half the wake diameter (see figure 1), i.e. a profile found close to the bluff body. For one of these profiles the usual critical Reynolds number has also been calculated with the result $R_c(\Lambda = -1, N = 3.2) = 9.1$. Although the assumption of quasi-parallel flow at such low Reynolds numbers is questionable, the result nevertheless shows that in the axisymmetric wake the range of convective instability between R_c and R_{cA} is much larger than in the two-dimensional wake (see Monkewitz 1988). This gives rise, under 'natural' excitation conditions commonly found in wind tunnels, to the observation of shear-layer modes (Achenbach 1974), associated with maximum spatial growth rate before helical vortex shedding becomes dominant.

That the nature of the instability for $R > R_{cA}$ is indeed absolute has been ascertained by verifying the pinching condition (see §2) in the k-plane. A representative example is shown as figure 4 at the minimum R_{cA}, $N = 3.2$ and $\Lambda = -1$ for which the pinching occurs at the real frequency $\omega^0 = 1.157$. It is evident that in this case the condition is satisfied as the branches $k^+(\omega)$ and $k^-(\omega)$ completely separate into the upper and lower half of the k-plane respectively when $\mathrm{Im}[\omega] = 0.68$.

For the comparison with experimental data on helical vortex shedding, more details of the instability characteristics have been determined for the $m = 1$ mode. On

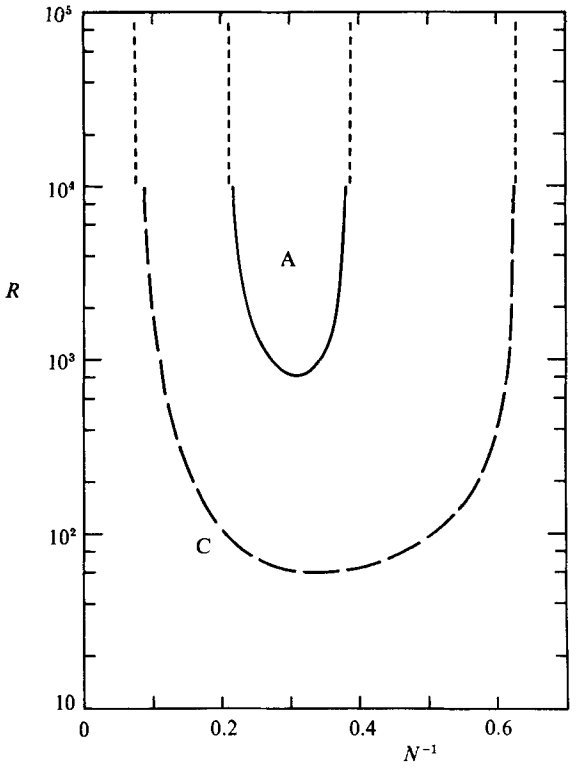

FIGURE 3. Absolute instability boundary in the (R, N^{-1})-plane for $\Lambda = -1$ (———) and $\Lambda = -1.1$ (— — —). – – – – – – –, asymptotes for $R \to \infty$. The regions of absolute and convective instability are indicated by A and C.

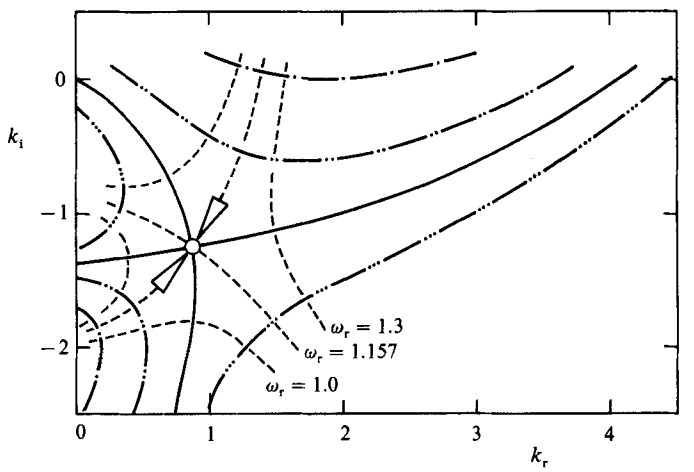

FIGURE 4. Maps $k(\omega)$ of contours parallel to the real axis of the ω-plane for the profile (1) with $\Lambda = -1$, $N = 3.2$ and $R = 820$. —·—·—, contour with $\mathrm{Im}[\omega] = 0.68$; —··—··—, $\mathrm{Im}(\omega) = +0.25$; ———, $\mathrm{Im}(\omega) = 0$; —···—···—, $\mathrm{Im}[\omega] = -0.25$; – – – – – – –, contours $\mathrm{Re}[\omega] =$ constant; ○, double root $k^+ = k^-$ at $\omega^0 = 1.157 + 0\mathrm{i}$. The pinching of the integration contour for the 'wavepacket integral' is indicated by arrows.

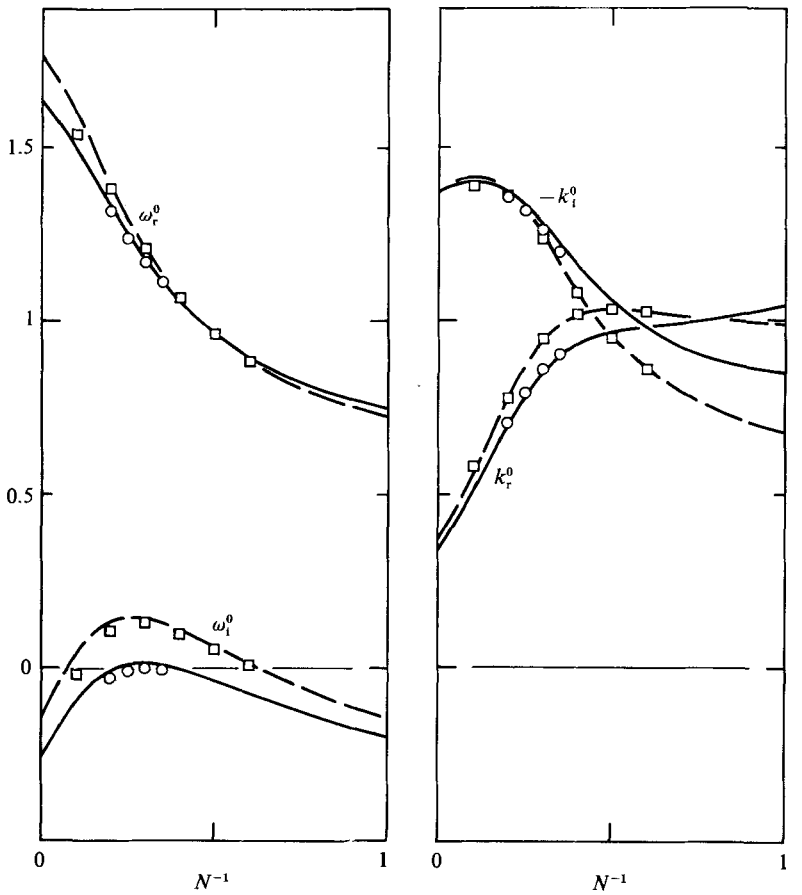

FIGURE 5. ω^0 and k^0 as a function of N^{-1} for: ———, $R = \infty$, $\Lambda = -1$; ○, $R = 1000$, $\Lambda = -1$; — — —, $R = \infty$, $\Lambda = -1.1$; □, $R = 1000$, $\Lambda = -1.1$.

figure 5 the location of the branch point ω^0 and the saddle point k^0 is plotted versus the profile shape parameter for $\Lambda = -1$ and $\Lambda = -1.1$ as well as the two Reynolds numbers of ∞ and 1000. This figure shows that, in the range of Reynolds numbers corresponding to the observed helical vortex shedding, it is primarily the velocity ratio that affects the stability characteristics. Furthermore, the quantity most affected by Λ is the absolute growth rate $\mathrm{Im}[\omega^0]$, while in all cases of this figure the real frequency $\mathrm{Re}[\omega^0]$, and the wavenumber k^0 appear well approximated by their values for $\Lambda = -1$ and $R = \infty$. These results conform with the physical intuition that reverse flow (i.e. $\Lambda < -1$) promotes absolute instability, i.e. enhances the growth of disturbances that travel upstream.

To relate these results to the more common stability calculations, the spatial instability characteristics have been computed for $\Lambda = -1$ and $R = \infty$ at both ends $N = 4.72$ and $N = 2.57$ of the absolutely unstable interval. Since for these two N the branch point ω^0 lies on the real axis, an infinite slope of $k(\omega)$ results there. This is shown on figure 6 where, for clarity, only the branches $k(\omega)$ are plotted that correspond to the regular (downstream) spatial branches in the adjoining convectively unstable regions. From this figure it becomes clear that the maximum spatial amplification is not necessarily attained at the branch-point frequency

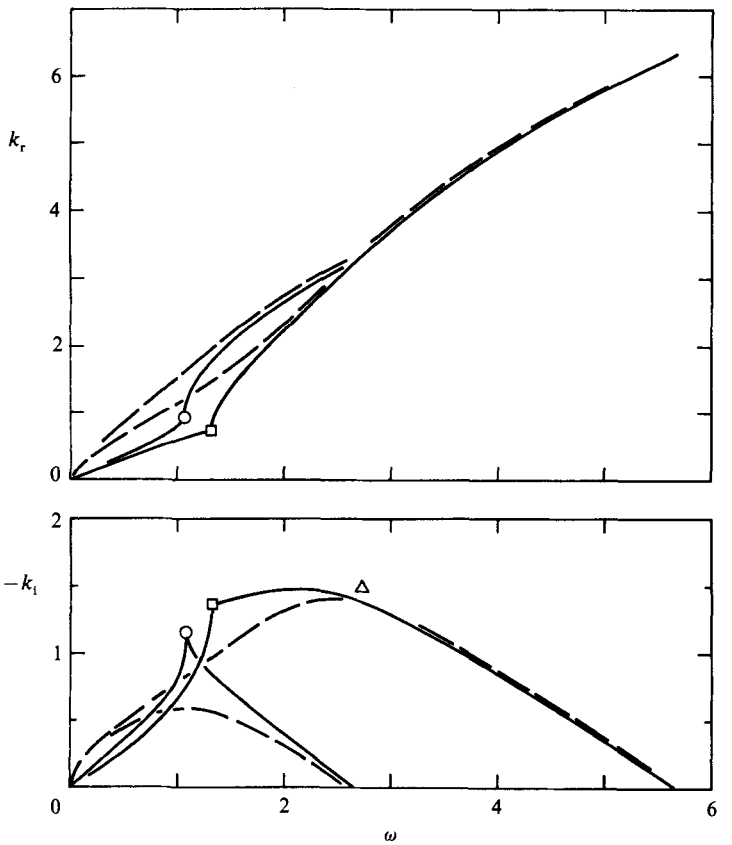

FIGURE 6. Spatial stability characteristics of the profile (1) for $\Lambda = -1$, $R = \infty$, and: ——○——, $m = 1$, $N = 2.57$; ——□——, $m = 1$, $N = 4.72$ with the symbols indicating the location of the saddle points k^0. ———, corresponding curves for $m = 0$; △, maximum spatial amplification of the two-dimensional hyperbolic tangent mixing layer with $\delta_\omega = [4.72 \ln 2]^{-1}$.

$\mathrm{Re}[\omega^0]$ (see also Monkewitz & Nguyen 1987, figure 9). For $N = 4.72$ the shear-layer mode associated with maximum spatial growth rate is clearly distinct from the mode with zero group velocity and in fact corresponds closely to Michalke's (1965) spatially most amplified mode in a plane hyperbolic tangent mixing layer (the comparison being made on the basis of equal vorticity thickness). In addition, figure 6 shows by comparison with the $m = 0$ mode that, as in the axisymmetric jet (Michalke 1971), the maximum spatial amplification of the shear-layer mode is virtually independent of the azimuthal wavenumber for low m-values and profiles with sufficiently thin mixing layers.

4. Summary and outlook

For the family of wake profiles under consideration with zero or near-zero centreline velocity a sequence of critical Reynolds numbers has been identified: first *the* critical Reynolds number R_c of the order of 10 at which the wake becomes convectively unstable. Then the occurrence of local absolute instability at an R_{cA} of the order of 10^2–10^3, depending on the amount of reverse flow (see figure 3), and

finally for a sphere wake, according to Achenbach's (1974) experiments, the onset of organized helical vortex shedding at approximately $R_{cH} = 1.5 \times 10^3$ in the present normalization. This sequence is identical to the one that leads to a self-excited global response in the model problem of Chomaz *et al.* (1988). Therefore a distinct possibility exists that the helical shedding from spheres and other axisymmetric bluff bodies represents such a self-excited response. It is noted though that in flow visualizations (e.g. Taneda 1978) the helical vortex structure is most clearly observed somewhat downstream of the body where the wake, according to the present results, is clearly convectively unstable. This is however not incompatible with the ideas put forward in this study since, pictorially speaking, the shedding may be imagined as being driven by a self-excited 'wavemaker' centred in the nearwake where the maximum slope thickness of the mixing layer is approximately 40–50% of the wake radius b^*.

To conclude this study, additional, albeit circumstantial, evidence is presented in support of the above hypothesis. First, it is noted that the most comprehensive Strouhal-number data on helical vortex shedding from spheres (Achenbach 1974, figure 3) show a trend with Reynolds number that is perfectly described by the relation $St_D = 0.19 - 400/R_D$, except in the transition region $2 \times 10^5 < R_D < 3 \times 10^5$. This is the same functional relation that has been proposed by Roshko (1953) for the Strouhal number of the Kármán vortex shedding behind circular cylinders, and that has been shown by Mathis *et al.* (1984) and Strykowski (1986) to be compatible with a self-excited global response governed by the Landau equation.

Next, as noted in §1, the results of Chomaz *et al.* (1988), the transient measurements of Mathis *et al.* (1984) and Strykowski (1986), and the relative success of the frequency selection criteria of Pierrehumbert (1984), Koch (1985) and Monkewitz & Nguyen (1987) in similar situations suggest that the present linear calculations may be useful for finding the approximate global response frequency. This is demonstrated by the final figure 7 which was obtained as follows. At each Reynolds number, the range of shape parameters N leading to absolute instability was determined for a fixed $\Lambda = -1$. The corresponding interval of real frequencies $\mathrm{Re}[\omega^0]$ then yielded a minimum and maximum response frequency at each Reynolds number, which, after conversion to a Strouhal number

$$St \equiv 2b^* f^* / U^*_{\max} = \mathrm{Re}[\omega^0]/((1-\Lambda)\pi),$$

defines the area of absolute instability on figure 7. Hence, all the Strouhal numbers within the area correspond to some local absolute instability in the wake, i.e. to some *growing* local mode with zero group velocity. At this point the choice of $\Lambda = -1$ requires some explanation since reverse flow undoubtedly occurs in the nearwake of axisymmetric bluff bodies. First it is observed that the range of $\mathrm{Re}\,[\omega^0]$ on figure 7, obtained for $\Lambda = -1$, closely corresponds, for $\Lambda < -1$, to the range of frequencies with maximum absolute growth rate $\mathrm{Im}\,[\omega^0]$ (see figure 5). The argument of Pierrehumbert (1984) and Chomaz *et al.* (1988), that the global response frequency is in many cases adequately approximated by the frequency of the local mode with zero group velocity and the largest $\mathrm{Im}\,[\omega^0]$, therefore serves as principal justification for using $\Lambda = -1$ in figure 7. Second, it may be added that the actual magnitude of the reverse flow is difficult to establish: while the data of Fail *et al.* (1959), Carmody (1964) and Riddhagni *et al.* (1971) yield minimum velocity ratios of between -1.9 and -2.4, Scholz (1986) obtains, with the pulsed hot-wire technique well adapted to reverse-flow regions, $\Lambda = -1.1$ one half-diameter downstream of a disk as opposed to $\Lambda = -1.5$ measured by Fail *et al.* at the same location.

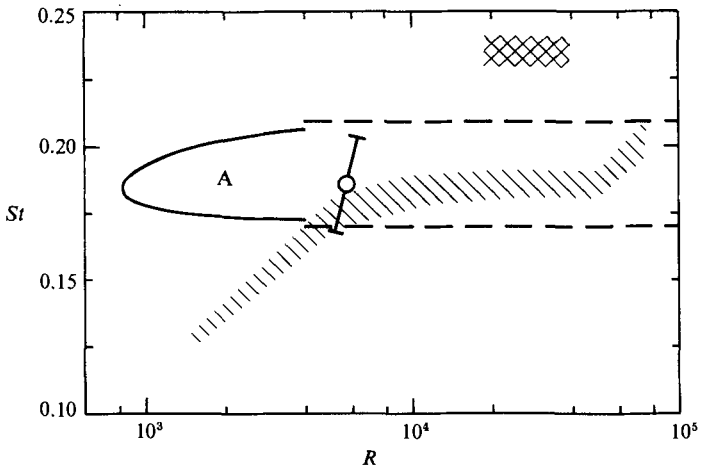

FIGURE 7. The range of absolutely unstable Strouhal numbers $St \equiv 2b^*f^*/U^*_{\max}$ for the profile family (1) with $A = -1$, as a function of Reynolds number. The area of absolute instability is marked by A. ———, asymptotes for $R \to \infty$; ○, data point of Scholz (1986) for a circular disk at $R_D = 1.5\ 10^4$; ▨, data of Achenbach (1974); ▨, data of Mair (1965).

To demonstrate the potential of local calculations for frequency estimates, different experimental data are superimposed on the theoretical results of figure 7. The first set of data is from Achenbach's (1974) figure 3. Lacking direct measurements, the conversion to the present normalization has been made on the basis of $A = -1$, i.e. $U^*_{\max} = 2\bar{U}^*$, and of the sphere diameter D^* being equal to the wake diameter $2b^*$. While this latter assumption appears justified at the higher Reynolds numbers where it yields an encouraging agreement with the linear calculations, it is, much as in the two-dimensional case (Monkewitz 1988), apparently poor near the onset of the vortex shedding.

A second data point has been obtained from Scholz's (1986) study of the wake behind a circular disk. The part of his results that is considered here may be summarized as follows. Besides distinct shear-layer modes approximately equally distributed between $m = 0$, 1, and 2 (his figure 14), he found between Reynolds numbers R_D, based on disk diameter and free-stream velocity, of 1.5×10^4 and 2×10^5 a strong $m = 1$ helical vortex shedding with a frequency about one order of magnitude below the shear-layer mode frequency (his figure 16). His measurements of the Strouhal numbers of the low-frequency helical mode are again compatible with the Roshko (1953) relationship between St and R. For the comparison with the present results only one data point was selected at $R_D = 1.5 \times 10^4$, where it was possible to obtain a good estimate of the ratio b^*/D^*. At about one diameter D^* downstream of the disk it was estimated from Scholz's flow visualization figures 10 and 11 to be between $b^*/D^* = 0.69$ and 0.83, yielding the error bar on figure 7. With the assumption of zero centreline velocity, i.e. $U^*_{\max} = 2\bar{U}^*$, good agreement is again obtained with the present stability calculations.

Finally, some interesting experiments of Mair (1965) are discussed in which he explored the effect of small disks placed downstream of a blunt-based body of revolution (a bullet). With a disk of diameter equal to 0.8 times the base diameter D^* placed at different distances from the base of the body, he found a critical distance of about $0.3D^*$ at which he observed sharply increased drag associated with

vigorous vortex shedding (without indicating the azimuthal wavenumber m). The reported Strouhal number for the cases of enhanced shedding are also included on figure 7, again using $A = -1$ and $b^*/D^* = 0.5$ for the conversion of normalizations. They are seen to fall somewhat high, which might possibly be due to a contraction of the wake over the low-pressure region between the base of the body and the smaller 'after-disk'. For disk positions further downstream up to a distance of $0.75D^*$ from the base, Mair found a drag reduction and less organized vortex shedding. This points to an intriguing possible explanation in terms of regions of absolute instability: With the control disk sufficiently far downstream of the body it may be that the wake beyond the disk is all convectively unstable with the postulated 'wavemaker' in the near wake either no longer self-excited owing to the altered boundary conditions, or effectively 'trapped' between the base and the disk. On the other hand, with the disk at the critical position for enhanced vortex shedding, it may provide a more favourable boundary condition for the global response to become self-excited than the base of the body.

This leads to the final observation that, in contrast to two-dimensional wakes where Kármán vortex shedding is virtually universal, the large-scale helical vortex shedding from axisymmetric bluff bodies appears quite sensitive to the boundary conditions, i.e. to the shape of the blunt body and in particular to the nature of the separation on the body (fixed by geometry or determined by the flow).

Appendix. The disturbance equations

In the following, $U(r)$ denotes the parallel mean flow velocity in the x-direction; $\hat{u}(r)$, $\hat{v}(r)$, and $\hat{w}(r)$ are the mode shapes of the disturbance velocities in the streamwise (x), radial (r), and azimuthal (θ) direction respectively; and $\hat{p}$ is the mode shape of the disturbance pressure (see equation (3) and note that the subscript m has been dropped in the following). For the inviscid calculations, the incompressible form (A 1) of Michalke's (1971) nonlinear first-order equation for the quantity χ is used:

$$\frac{\mathrm{d}\chi}{\mathrm{d}r} = \chi^2 \frac{1+(m/kr)^2}{U-c} + \chi\left[\frac{1}{r} - \frac{\mathrm{d}U/\mathrm{d}r}{U-c}\right] - k^2(U-c), \qquad \text{(A 1)}$$

$$\chi \equiv -\frac{\mathrm{i}k\hat{p}}{\hat{v}}.$$

The boundary conditions on the wake centreline (A 2) and at infinity (A 3) are obtained by solving (A 1) for $\mathrm{d}U/\mathrm{d}r = 0$ with the additional requirements that all physical disturbance quantities are non-singular on the centreline and vanish at infinity:

$$\chi \approx -k[U(0)-c]\frac{I_m(kr)}{I'_m(kr)}, \quad r \to 0, \qquad \text{(A 2)}$$

$$\chi \sim -k[U(\infty)-c]\frac{K_m(kr)}{K'_m(kr)}, \quad r \to \infty, \qquad \text{(A 3)}$$

Above, I_m and K_m are the modified Bessel functions of the first and second kind of order m, and a prime denotes a derivative with respect to the argument. For the viscous calculations, the set of equations (A 4) was used. It is essentially the same as the one derived in detail by Morris (1976) and is the equivalent, in cylindrical

coordinates and in primitive variables, of the standard Orr–Sommerfeld equation plus the transverse momentum equation for three-dimensional normal modes:

$$\frac{\mathrm{d}}{\mathrm{d}r}\begin{pmatrix} \hat{f} \\ \mathrm{D}\hat{f} \\ \hat{g} \\ \hat{u} \\ \mathrm{D}\hat{u} \\ \hat{p}\,\mathrm{R} \end{pmatrix} = \begin{pmatrix} 0 & 1 & 0 & 0 & 0 & 0 \\ \left(\frac{\kappa^2}{2}+\frac{m+1}{r^2}\right) & \left(-\frac{m+1}{r}\right) & \left(-\frac{\kappa^2}{2}\right) & \left(-\frac{\mathrm{i}km}{r}\right) & (-\mathrm{i}k) & \left(-\frac{m}{r}\right) \\ \left(-\frac{m+1}{r}\right) & -1 & \left(\frac{m-1}{r}\right) & (-2\mathrm{i}k) & 0 & 0 \\ 0 & 0 & 0 & 0 & 1 & 0 \\ \left(\frac{1}{2}\frac{\mathrm{d}U}{\mathrm{d}r}\mathrm{R}\right) & 0 & \left(\frac{1}{2}\frac{\mathrm{d}U}{\mathrm{d}r}\mathrm{R}\right) & \left(\kappa^2+\frac{m^2}{r^2}\right) & \left(-\frac{1}{r}\right) & (\mathrm{i}k) \\ \left(-\frac{\kappa^2}{2}-\frac{m(m+1)}{r^2}\right) & \left(-\frac{m}{r}\right) & \left(-\frac{\kappa^2}{2}\right) & \left(-\frac{\mathrm{i}km}{r}\right) & (-\mathrm{i}k) & 0 \end{pmatrix} \begin{pmatrix} \hat{f} \\ \mathrm{D}\hat{f} \\ \hat{g} \\ \hat{u} \\ \mathrm{D}\hat{u} \\ \hat{p}\,\mathrm{R} \end{pmatrix}, \tag{A 4}$$

$$\kappa^2 \equiv k^2 + \mathrm{i}k\,\mathrm{R}\,[U(r)-c],$$

$$\hat{f} \equiv \hat{u} + \mathrm{i}\hat{w}, \quad \hat{g} \equiv \hat{u} - \mathrm{i}\hat{w}.$$

The same physical boundary conditions as in the inviscid case lead to three linearly independent starting solutions each near the centreline (A 5) and far away from the wake (A 6):

$$\begin{pmatrix} \hat{f} \\ \mathrm{D}\hat{f} \\ \hat{g} \\ \hat{u} \\ \mathrm{D}\hat{u} \\ \hat{p} \end{pmatrix} \approx \begin{pmatrix} I_{m+1}(kr) \\ kI'_{m+1}(kr) \\ I_{m-1}(kr) \\ \mathrm{i}I_m(kr) \\ \mathrm{i}kI'_m(kr) \\ -\mathrm{i}(U-c)I_m(kr) \end{pmatrix}, \begin{pmatrix} kI_{m+1}(\kappa r) \\ k\kappa I'_{m+1}(\kappa r) \\ 0 \\ \frac{\mathrm{i}\kappa}{2}I_m(\kappa r) \\ \frac{\mathrm{i}\kappa^2}{2}I'_m(\kappa r) \\ 0 \end{pmatrix}, \begin{pmatrix} 0 \\ 0 \\ kI_{m-1}(\kappa r) \\ \frac{\mathrm{i}\kappa}{2}I_m(\kappa r) \\ \frac{\mathrm{i}\kappa^2}{2}I'_m(\kappa r) \\ 0 \end{pmatrix}, \quad r \to 0 \tag{A 5}$$

$$\begin{pmatrix} \hat{f} \\ \mathrm{D}\hat{f} \\ \hat{g} \\ \hat{u} \\ \mathrm{D}\hat{u} \\ \hat{p} \end{pmatrix} \sim \begin{pmatrix} -K_{m+1}(kr) \\ -kK'_{m+1}(kr) \\ -K_{m-1}(kr) \\ \mathrm{i}K_m(kr) \\ \mathrm{i}kK'_m(kr) \\ -\mathrm{i}(U-c)K_m(kr) \end{pmatrix}, \begin{pmatrix} -kK_{m+1}(\kappa r) \\ -k\kappa K'_{m+1}(\kappa r) \\ 0 \\ \frac{\mathrm{i}\kappa}{2}K_m(\kappa r) \\ \frac{\mathrm{i}\kappa^2}{2}K'_m(\kappa r) \\ 0 \end{pmatrix}, \begin{pmatrix} 0 \\ 0 \\ -kK_{m-1}(\kappa r) \\ \frac{\mathrm{i}\kappa}{2}K_m(\kappa r) \\ \frac{\mathrm{i}\kappa^2}{2}K'_m(\kappa r) \\ 0 \end{pmatrix}, \quad r \to \infty. \tag{A 6}$$

REFERENCES

ACHENBACH, E. 1972 Experiments on the flow past spheres at very high Reynolds numbers. *J. Fluid Mech.* **54**, 565.

ACHENBACH, E. 1974 Vortex shedding from spheres. *J. Fluid Mech.* **62**, 209.

BECHERT, D. 1985 Excitation of instability waves. *Z. Flugwiss, Weltraumforschung* **9**, 356.

BERS, A. 1975 Linear waves and instabilities. In *Plasma Physics* (ed. C. DeWitt & J. Peyraud), p. 113. Gordon & Breach.

BRIGGS, R. J. 1964 *Electron Stream Interaction with Plasmas.* M.I.T. Press.

CARMODY, T. 1964 Establishment of the wake behind a disk. *Trans. ASME* D: *J. Basic Engng* **86**, 869.

CHOMAZ, J. M., HUERRE, P. & REDEKOPP, L. G. 1988 Bifurcations to local and global modes in spatially developing flow. *Phys. Rev. Lett.* **60**, 25.

DEISSLER, R. J. 1987 The convective nature of instability in plane Poiseuille flow. *Phys. Fluids* **30**, 2303.

FAIL, R., LAWFORD, J. A. & EYRE, R. C. W. 1959 Low-speed experiments on the wake characteristics of flat plates normal to an air stream. *Aero. Res. Council R & M* 3120.

HUERRE, P. 1987 Spatio-temporal instabilities in closed and open flows. In *Instabilities and Nonequilibrium Structures* (ed. E. Tirapegui & D. Villarroel), p. 141. Reidel.

HUERRE, P. & MONKEWITZ, P. A. 1985 Absolute and convective instabilities in free shear layers. *J. Fluid Mech.* **159**, 151.

ILEGBUSI, J. O. & SPALDING, D. B. 1984 A steady-unsteady visualization technique for wake-flow studies. *J. Fluid Mech.* **139**, 435.

KOCH, W. 1985 Local instability characteristics and frequency determination of self-excited wake flows. *J. Sound & Vib.* **99**, 53.

LIFSHITZ, E. M. & PITAEVSKII, L. P. 1981 *Physical Kinetics*, paragraph 62. Pergamon.

MAIR, W. A. 1965 The effect of a rear-mounted disc on the drag of a blunt-based body of revolution. *Aero Q.* **16**, 350.

MATHIS, C., PROVANSAL, M. & BOYER, L. 1984 The Bénard–von Kármán instability: an experimental study near the threshold. *J. Phys. Lett.* **45**, L-483.

MICHALKE, A. 1965 On spatially growing disturbances in an inviscid shear layer. *J. Fluid Mech.* **23**, 521.

MICHALKE, A. 1971 Instabilität eines kompressiblen runden Freistrahls unter Berücksichtigung des Einflusses der Strahlgrenzschichtdicke. *Z. Flugwiss.* **19**, 319.

MONKEWITZ, M. A. 1978 Analytic pseudoorthogonalization methods for linear two-point boundary value problems illustrated by the Orr–Sommerfeld equation. *Z. Angew. Math. Phys.* **29**, 861.

MONKEWITZ, P. A. 1988 The absolute and convective nature of instability in two-dimensional wakes at low Reynolds numbers. *Phys. Fluids* (to appear).

MONKEWITZ, P. A. & NGUYEN, L. N. 1987 Absolute instability in the near-wake of two-dimensional bluff bodies. *J. Fluids Structures* **1**, 165.

MONKEWITZ, P. A. & SOHN, K. D. 1986 Absolute instability in hot jets and their control. *AIAA paper* 86–1882.

MORRIS, P. J. 1976 The spatial viscous instability of axisymmetric jets. *J. Fluid Mech.* **77**, 511.

PAO, H. P. & KAO, T. N. 1977 Vortex structure in the wake of a sphere. *Phys. Fluids* **20**, 187.

PIERREHUMBERT, R. T. 1984 Local and global baroclinic instability of zonally varying flows. *J. Atmos. Sci.* **41**, 2141.

RIDDHAGNI, P. R., BEVILAQUA, P. M. & LYKOUDIS, P. S. 1971 Measurements in the turbulent wake of a sphere. *AIAA J.* **9**, 1433.

ROSHKO, A. 1953 On the development of turbulent wakes from vortex streets. *NACA Tech. Note* 2913.

SATO, H. & OKADA, O. 1966 The stability and transition of an axisymmetric wake. *J. Fluid Mech.* **26**, 237.

SCHLICHTING, H. 1968 *Boundary-Layer Theory*, 6th edn. McGraw Hill.

SCHOLZ, D. 1986 Kohärente Wirbelstrukturen im Nachlauf einer ruhenden und einer schwingungserregten Kreisscheibe. *Res. rep.* DFVLR-FB-86-04.

STRANGE, P. J. R. & CRIGHTON, D. G. 1983 Spinning modes in axisymmetric jets. *J. Fluid Mech.* **134**, 231.

STRYKOWSKI, P. J. 1986 The control of absolutely and convectively unstable shear flows. Ph.D. thesis, Yale University.

TANEDA, S. 1978 Visual observation of flow past a sphere at Reynolds numbers between 10^4 and 10^6. *J. Fluid Mech.* **85**, 187.

TOROBIN, L. B. & GAUVIN, W. H. 1959 Fundamental aspects of solid–gas flow. Part II. The sphere wake in steady laminar fluids. *Can. J. Chem. Engng* **37**, 167.